SHIMADZU
Excellence in Science

Application Note

No. 74

Additive manufacturing

Effects of Defects in Very High Cycle Fatigue of Additively Manufactured AlSi12

Mustafa Awd, Frank Walther*1

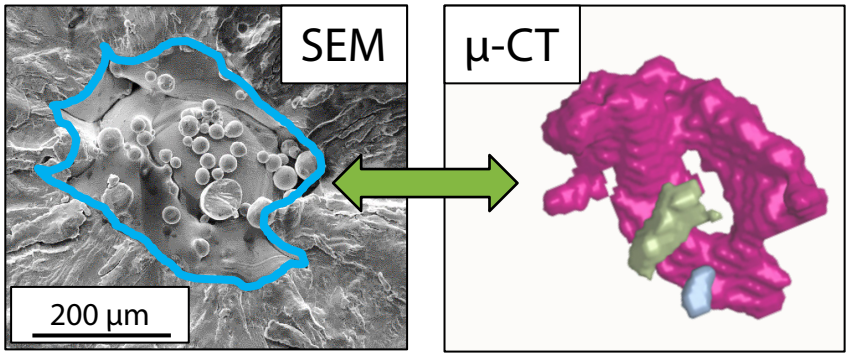

Correlation between scanning electron microscopy and microcomputed tomography

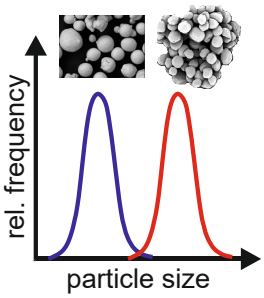

Powder particle size distribution

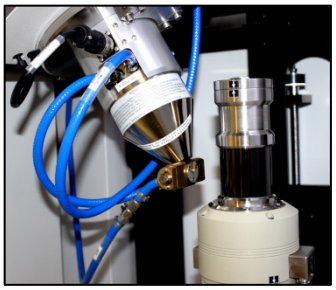

In-situ X-ray scanning

Additive manufacturing

1. Introduction

Currently, research is focusing on the reliability of materials and structures. In comparison to other methods of metal additive manufacturing (AM), selective laser melting (SLM) is an efficient powder bed-based metal AM technology [1), 2)]. To estimate the required quality of SLM components, fatigue-related problems must be investigated [3), 4), 5)]. Aluminum is used in a broad number of applications, the most notable of which are in the automotive and aerospace industries. Aluminum-silicon alloys are well-established in SLM processing, with AlSi12, AlSi10Mg, and Scalmalloy® being routinely treated. SLM processing took use of the Si content's influence on increasing strength till a eutectic point was reached. Simultaneously, the eutectic composition makes the SLM processing of aluminum alloys more favorable [6), 7), 8)].

The fatigue strength of SLM-manufactured alloys was found to be like or greater than that of cast alloys, e.g. [9), 10), 11)], with a few outliers [12), 13)]. The most significant element is the effect of the small porosity and nonuniform behavior of SLM-processed components during fatigue. Brandl et al. [9)] investigated AlSi10Mg subjected to high cycle fatigue (HCF) loading through SLM. Three different orientations of the platform, 0˚, 45˚, and 90˚, were manufactured and tested in two conditions: as-built and peak hardened. Due to the variety of types of porosity, predicting the fatigue life of SLM components is essential.

This article explores the relationship between the production process, the structure, and the properties of AlSi12 alloy in detail. The research was undertaken to determine the effect of process variables on the microstructure features. Mechanical properties ranging from hardness and quasi-static behavior to very high cycle fatigue (VHCF) behavior have been investigated. The damage processes in HCF and VHCF areas using the morphology of internal defects and microstructural features were analyzed. The findings may be utilized to develop a cumulative approach for controlling the SLM process parameters required for the desired microstructure and for calculating residual porosity to properly predict mechanical behavior under fatigue loading.

*1 Chair of Materials Test Engineering (WPT), TU Dortmund University, Baroper Str. 303, 44227 Dortmund, Germany

2. Materials and Equipment

The goal is to compare the effect of relative density content on damaging processes when VHCF loading is applied. The specimens were processed using standard PBF-LB settings. The platform was warmed to 200 ˚C using SLM-AutoFabCAM software, the melting pools were shielded with Argon gas, and the chessboard strategy island hatching was employed. The vector orientation plane was rotated by 79˚ each layer during contour hatching [14].

The ultrasonic fatigue (USF) testing equipment from Shimadzu (USF-2000A, Fig. 1) was utilized to conduct VHCF testing using the testing configuration indicated in Fig. 2. The actuator is based on the piezoelectric principle, which resonates at a frequency of 20 kHz when just one end of the specimen is powered, and the other remains unclamped. A horn transmits the vibrations to the specimen. They are constructed in such a way that they transfer resonant longitudinal waves through the solid bodies, increasing displacement at the specimen's free end and stress at the specimen's center. Since utilizing high frequencies causes the specimen to heat up, tests were done using intermittent vibrations with a pulse:pause ratio of 50:50. The system was meant to experience resonance for 200 ms and then to shut down for the next 200 ms. Additionally, during testing, air cooling was used. As a result, the temperature increase induced by stress and frequency was limited to fewer than 10 K. Shimadzu HMV-G21 equipment was used to conduct microhardness testing and distributions of microhardness.

Fig. 1 Shimadzu USF-2000A

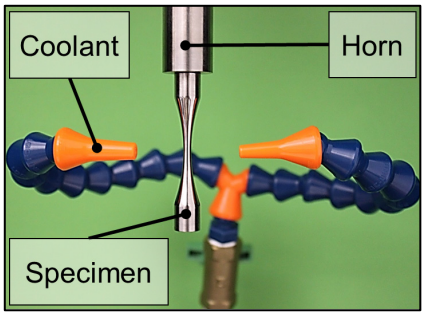

Fig. 2 Cooling nozzles during vibration [14]

3. Results

The load increase test (LIT) was utilized in Fig. 3 to distinguish the LCF, HCF, and VHCF fatigue regimes. In HCF, plasticity is mostly microscale and limited to a few grains. At comparable stress amplitudes, there is no evidence of macroscopic irreversible cyclic plasticity. According to the plastic strain response, the maximum stress amplitude for this class of alloys is 100 MPa. This amount of stress amplitude marks the boundary between the HCF and VHCF regions. When the specimen approaches plastic saturation at 150 MPa amplitude, uniform macroscopic plastic deformation occurs. Stress-relief treatment led to a more consistent AlSi12 (A–B) response [14], which allows for the ignoring of the failure stress amplitude difference. Consistently, batch A accumulated a greater amount of irreversible plastic strain than batch B.

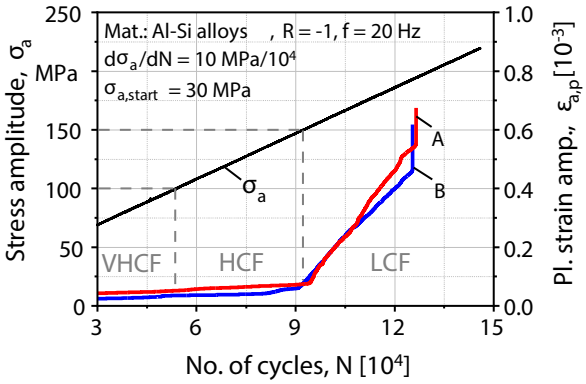

Batch	Alloy	PH	SR [2 hrs]
A	AlSi12	./.	240 ˚C
B	AlSi12	200 ˚C	240 ˚C

PH: Platform heating, **SR**: Stress relieved

Fig. 3 Accumulation of plastic strain of AlSi12 batches A [SR] and B [PH+SR] [14]

In the direction of the cooling gradient, the AlSi12 morphology is equiaxed cellular dendritic rather than longitudinal columnar dendritic. The influence of platform heating (PH) is seen in Figs. 4a and 4c, even though both specimens were relieved (SR). Thickening of dendritic walls was observed. Saturated Si resulted in the formation of larger aggregates. The Z-plane exhibits a greater degree of dendritic wall thickening.

Without the presence of PH in the Z-plane, batch B exhibits a more solid texture.

As a result, the microstructure loses some of its anisotropy. Almost everything about the cooling gradients and solidification direction is revealed by the microstructure. The achieved strength is mostly determined by the grain fineness and supersaturation of Si particles in the Al matrix.

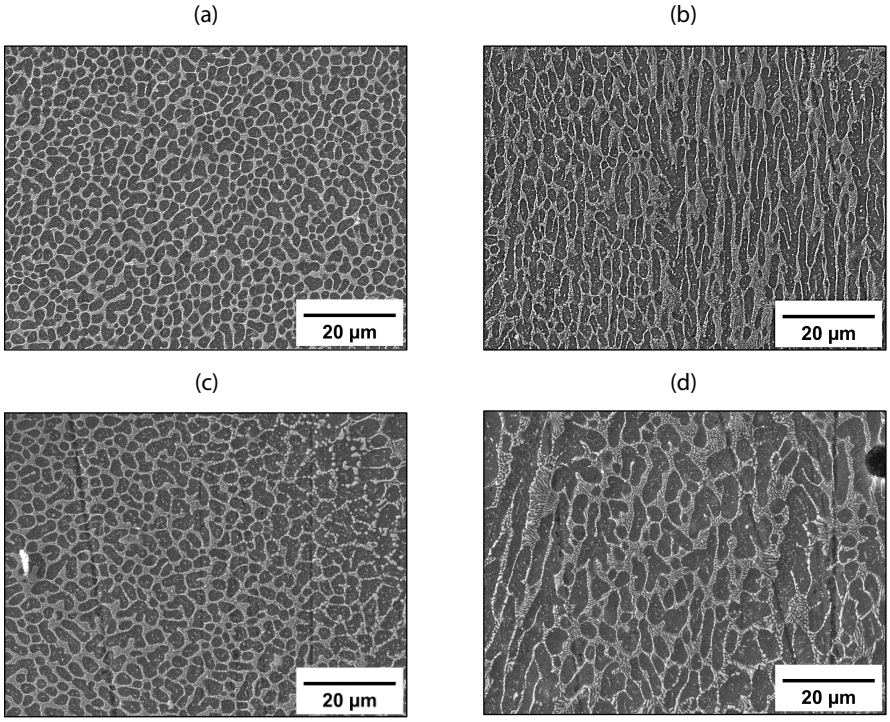

Fig. 4 Influence of platform heating (PH) in AlSi12 batches A [SR] and B [PH+SR] under scanning electron microscopy: a) Batch A (XY-section), b) batch A (Z-section), c) batch B (XY-section), d) batch B (Z-section) [14)]

Nondestructive X-ray microcomputed tomography (µ-CT) testing was used to estimate the volumetric pore fraction. Volumetric tomography is illustrated in Figs. 5a and 5b. The density fractions of these samples from µ-CT were 99.75 and 99.88 %, respectively. The pore fraction obtained by µ-CT is often somewhat smaller than the pore fraction found by metallographic image analysis. This pattern is compatible with what has been found in metallographic investigations, namely, a reduction in porosity because of platform heating. µ-CT examines the entire internal structure of the material, making it more reliable than 2D-metallography, which is based on the sliced section. Fig. 5 illustrates that when the platform is heated in batch B, a consistent reduction in the frequency of pores is achieved. Individual rods of Mg2Si have been seen at remelting locations in a less cohesive fashion.

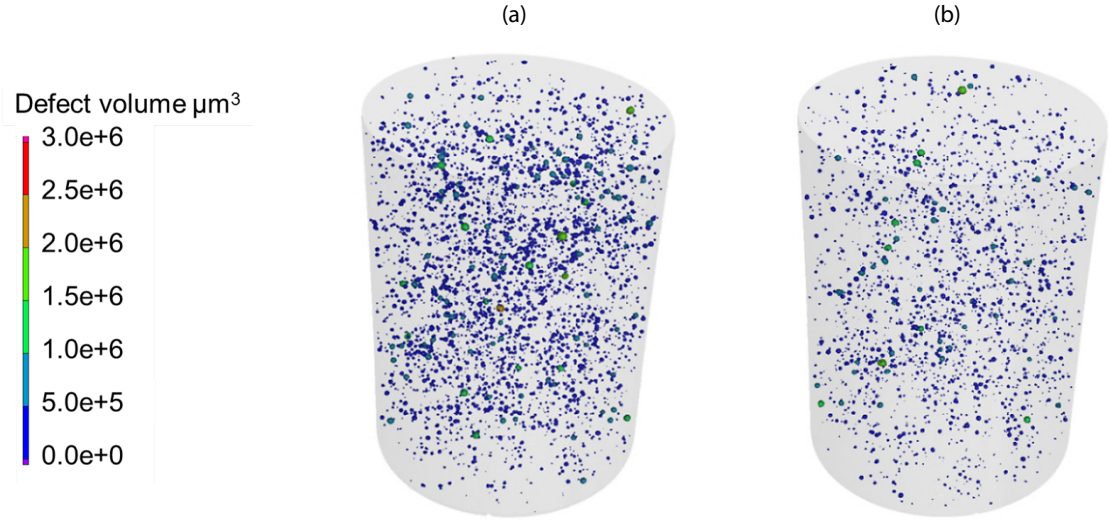

Fig. 5 3D µ-computed tomography defect analysis of batches A [SR] and B [PH+SR] [11)]

The microstructure refinement of AlSi12 influences its microhardness. AlSi12 batch B, as seen in Fig. 6, has a lower hardness value than batch A. This difference is due to their distinct thermal histories. Due to the presence of PH, the cooling rate was slowed, resulting in the initial partial segregation of Si along grain boundaries. As a result, following PH, fewer early diffusion sites were found.

On the other hand, prior to SR, a greater number of beginning sites were discovered due to the absence of PH, which results in higher Si particle saturation levels. This decrease is consistent with the decreased cooling rates seen in the microstructure and residual stress profiles associated with it.

The impact of platform heating and post-process stress reduction was shown to be statistically significant at a significance level of 0.05.

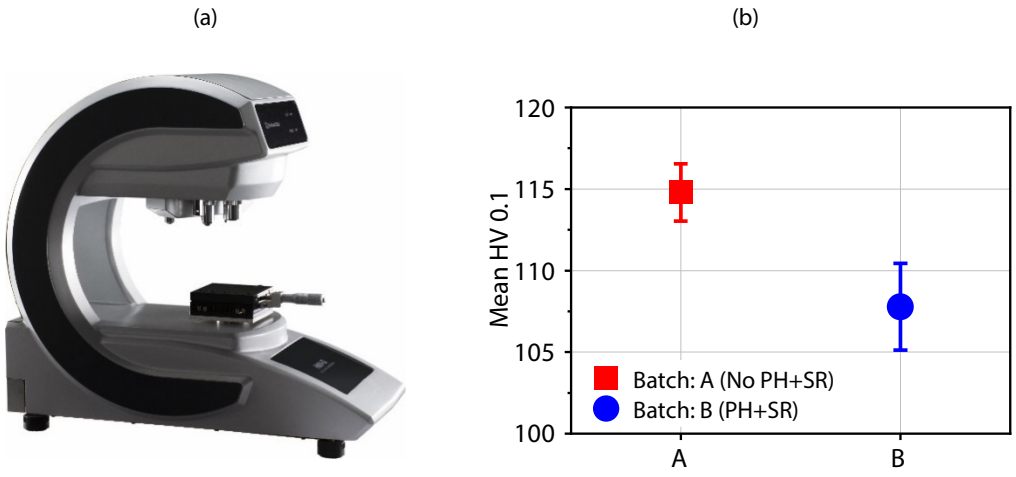

Fig. 6 a) Shimadzu HMV-G hardness tester, b) influence of Si content and microstructural features on micro-hardness properties of AlSi12 batches A [SR] and B [PH+SR] [11)]

The entire Woehler curve is depicted in Fig. 7, including the high cycle fatigue (HCF) and very high cycle fatigue (VHCF) sections. The fatigue strength of batch B specimens (with platform heating) is higher than that of batch A specimens at 1E9 cycles (without platform heating). The trend is not continuous; batch A has a higher fatigue strength than batch B for larger stress amplitudes, but the trend reverses at 120 MPa. This phenomenon occurs because of the interaction between microstructure and process-induced defects (flaws) under a variety of stress-raising situations. As with HCF, the fatigue strength of a material is dictated by its resistance to fracture initiation, which is stronger in fine grains.

On a microstructural level, its smaller dendritic width may account for the specimen's extended life at 140 MPa without platform heating. The other crucial point is the difference in residual porosity between the two batches. These pores remain relatively passive under lower stresses, implying that a coarser microstructure has a proportionally longer fatigue life than a finer microstructure during the fracture propagation phase. The results suggest that platform heating influences fatigue life that is likewise proportional to the level of the applied load.

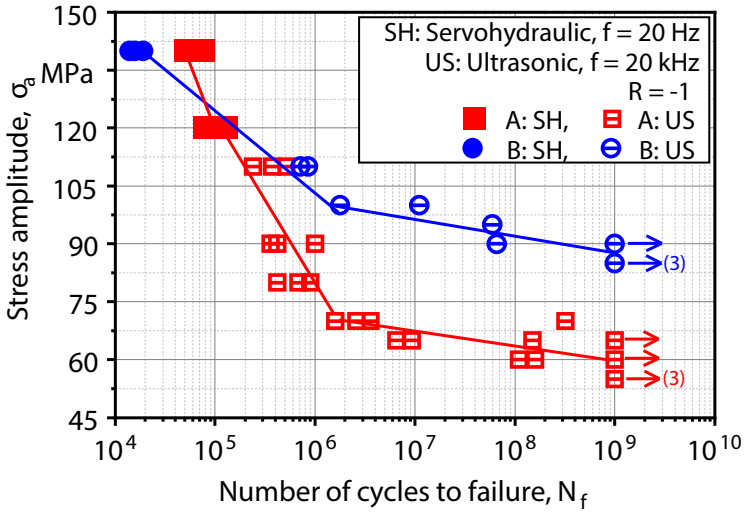

Fig. 7 S-N (Woehler) curves of AlSi12 batches A [SR] and B [PH+SR], results determined with servohydraulic (20 Hz) and ultrasonic (20 kHz) testing until VHCF range [11)]

Figs. 8a and 8b illustrate the crack-initiating pores in batch A. Due to the irregular shape and internal notch morphology, the defect size is three times larger, resulting in a significantly reduced fatigue life, even at 70 MPa stress amplitude.

At 1E5 cycles, the fatigue strength inequality is considerably reduced in the HCF regime. The finer microstructure of batch A retards fatigue crack development, therefore delaying fracture.

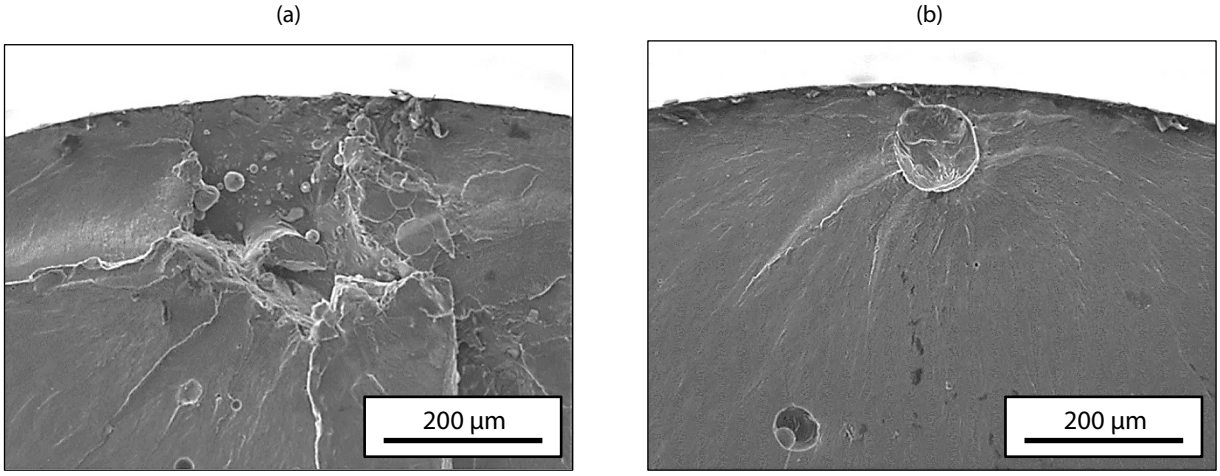

Fig. 8 Fractographic identification of crack initiation side for (a) batch A [SR] at 70 MPa and N_f = 1.6E6 and (b) batch A [SR] at 70 MPa and N_f = 3.2E8 [11)]

In both batches, a failure is envisioned, which is initiated by a subsurface pore. Since these samples were not built near-net-shape but were machined to their final geometries, the bulk internal porosity is brought closer to the surface.

An undesirable combination of planar stress concentrations and crystallographic orientations surrounding the pores facilitates the separation of pores at their mid planes. Multiple crack initiations coalescence resulted in batch A experiencing an expedited failure and reduced fatigue strength.

4. Summary

For additively manufactured (AM) alloy AlSi12, the influence of process-induced porosity on the fatigue life and limit was studied. In HCF and VHCF regimes, porosity resulted in a shorter fatigue lifespan. In the LCF area, platform heating lowers fatigue life at higher loads but increases it in the HCF and VHCF regimes. VHCF testing was conducted using Shimadzu's ultrasonic fatigue (USF) testing equipment. Intermittent vibrations with a pulse:pause ratio of 50:50 were used in the experiments. Using selected fractographic tests, the defect-specific fatigue failure of AM aluminum alloys may be precisely determined and validated. Mechanical fracture analysis of defects in AM aluminum-silicon alloys enables a reliable estimate of the fatigue life and limit of fine AM microstructures by considering the unique pore distributions.

Relevant previous application notes:

- **SCA-300-071**: USF-2000A - Damage Mechanism Separation in Very High Cycle Fatigue of Additively Manufactured AlSi12 and DieCast AlSi7Mg0.3 https://www.shimadzu.eu/SCA-300-071

- **SCA-300-001**: Very High Cycle Fatigue (VHCF) Assessment of Laser Additive Manufactured (LAM) AlSi12 Alloy https://www.shimadzu.eu/sites/shimadzu.seg/files/SEG-images/EUIC/composite/SCA_300_001_Application_190214_VHCF_USF2000.pdf

Further research papers of the authors:

- https://wpt.mb.tu-dortmund.de/en/research/publications/

<References>

1) Frazier, W.: Metal additive manufacturing: A review. Journal of Materials Engineering and Performance 23, 6 (2014) 1917–1928.
2) Campbell, I.; Bourell, D.; Gibson, I.: Additive manufacturing: Rapid prototyping comes of age. Rapid Prototyping Journal 18, 4 (2012) 255–258.
3) Bremen, S.; Meiners, W.; Diatlov, A.: Selective laser melting: A manufacturing technology for the future? Laser Technik Journal 9, 2 (2012) 33–38.
4) Lewandowski, J.; Seifi, M.: Metal additive manufacturing: A review of mechanical properties. Annual Reviews of Materials Research 46 (2016) 151–186.
5) Ngnekou, J.D.; Nadot, Y.; Henaff, G.; Nicolai, J.; Haokan, W.; Cairney, J.; Ridosz, L.: Fatigue properties of AlSi10Mg produced by additive layer manufacturing. International Journal of Fatigue 119 (2019) 160–172.
6) Prashanth, K.; Scudino, S.; Klauss, H.; Surreddi, K.; Löber, L.; Wang, Z.; Chaubey, A.; Kühn, U.; Eckert, J.: Microstructure and mechanical properties of Al-12Si produced by selective laser melting: Effect of heat treatment. Materials Science and Engineering A 590 (2014) 153–160.
7) Buchbinder, D.; Meiners, W.; Wissenbach, K.; Poprawe, R.: Selective laser melting of aluminum diecast alloy – Correlations between process parameters, solidification conditions, and resulting mechanical properties. Journal of Laser Applications 27 (2015) S2.
8) Awd, M.; Tenkamp. J.; Hirtler, M.; Siddique, S.; Bambach, M.; Walther, F.: Comparison of microstructure and mechanical properties of Scalmalloy® produced by selective laser melting and laser metal deposition. Materials 111 (2018) 1–17.
9) Siddique, S.; Imran, M.; Wycisk, E.; Emmelmann, C.; Walther, F.: Influence of process-induced microstructure and imperfections on mechanical properties of AlSi12 processed by selective laser melting. Journal of Materials Processing Technology 221 (2015), 205–213.
10) Brandl, E.; Heckenberger, U.; Holzinger, V.; Buchbinder, D.: Additive manufactured AlSi10Mg samples using selective laser melting (SLM): Microstructure, high cycle fatigue, and fracture behavior. Materials and Design 34 (2012) 159–169.
11) Siddique, S.; Imran, M.; Walther, F.: Very high cycle fatigue and fatigue crack propagation behavior of selective laser melted AlSi12 alloy. International Journal of Fatigue 94, 2 (2017) 246–254.
12) Bagherifard, S.; Beretta, N.; Monti, S.; Riccio, M.; Bandini, M.; Guagliano, M.: On the fatigue strength enhancement of additive manufactured AlSi10Mg parts by mechanical and thermal post-processing. Materials and Design 145 (2018) 28–41.
13) Tang, M.; Pistorius, P.: Oxides porosity and fatigue performance of AlSi10Mg parts produced by selective laser melting. International Journal of Fatigue 94, 2 (2017) 192–201.
14) Awd, M.; Siddique, S.; Walther, F.: Microstructural damage and fracture mechanisms of selective laser melted Al-Si alloys under fatigue loading. Theoretical and Applied Fracture Mechanics 106 (2020) 102483.

First Edition: Feb. 2022

SHIMADZU
Shimadzu Corporation
Analytical & Measuring Instruments Division
Global Application Development Center

www.shimadzu.com/an/

› Please fill out the survey

Related Products Some products may be updated to newer models.

› USF-2000A
Ultrasonic Fatigue Testing System

Related Solutions

› Metal

› Price Inquiry

› Product Inquiry

› Technical Service / Support Inquiry

› Other Inquiry